Rad9B responds to nucleolar stress through ATR and JNK signalling, and delays the G1–S transition

Antonio Jesús Pérez-Castro and Raimundo Freire*

Unidad de Investigación, Hospital Universitario de Canarias, Instituto de Tecnologías Biomédicas, Ofra s/n, La Laguna, Tenerife, Spain

*Author for correspondence (rfreire@ull.es)

Accepted 8 November 2011
Journal of Cell Science 125, 1152–1164

doi: 10.1242/jcs.091124

Summary

The complex formed by Rad9, Rad1 and Hus1 (9-1-1) protects against genomic instability by activating DNA damage checkpoint and DNA damage repair pathways, mainly in response to replication fork collapse and UV lesions. Here we compare the role of Rad9A (also known as Rad9) with the human paralogue Rad9B. Unlike Rad9A, overexpression of Rad9B delays cells in G1 phase. Moreover, Rad9B migrates to nucleoli after nucleolar stress in an ATR- and JNK-dependent manner, in a newly described nucleolar domain structure containing p21. Analysis of chimeras of Rad9A and Rad9B demonstrate that localisation to nucleoli and the block in G1 phase upon overexpression crucially depend on the Rad9B C-terminal tail. Taken together, data presented here show a relationship between Rad9B and pathways for checkpoints, stress response and nucleolar function.

Key words: Rad9B, ATR, JNK, Nucleolar stress, 9-1-1

Introduction

Different DNA aberrant structures, such as stalled replication forks or UV-modified bases, challenge cell viability and genomic stability and trigger cellular DNA damage responses (DDRs) in which, in higher eukaryotes, the kinase ATR [ataxia telangiectasia mutated (ATM)- and RAD3-related)] plays a role. ATR is extensively reported to be required for the DNA damage checkpoint and its activation depends on replication protein A (RPA)-coated ssDNA regions, that are formed upon damage directly or after the damaged DNA has been processed (Zou and Elledge, 2003). To activate the DNA damage checkpoint, ATR needs the contribution of other factors such as the 9-1-1 complex, Rad17 and TopBP1. The 9-1-1 heterotrimeric complex is formed by Rad9A, Rad1 and Hus1, and shares homology with homotrimeric proliferating cell nuclear antigen (PCNA), including its ring structure (Dore et al., 2009). In response to UV radiation or stalled replication, 9-1-1 is loaded onto the chromatin on the sites of damage by the Rad17–RFC (replication factor C) complex, which opens the 9-1-1 structure and allows it to embrace the DNA (Rauen et al., 2000). The accumulation of the 9-1-1 complex at sites of DNA lesions can be visualised by nuclear foci (Medhurst et al., 2008). Loading of 9-1-1 facilitates the recruitment of ATR activator TopBP1, which binds the phosphorylated C-terminal tail of Rad9A (Delacroix et al., 2007). ATR is then able to phosphorylate the effector kinase Chk1 in a claspin-dependent manner (Wang et al., 2006).

MAPK pathways are activated by UV lesions, and cross-relationships with the ATR–Chk1 pathway are described. For example, ATR can trigger the JNK pathway by phosphorylation of Jun (Foray et al., 2003) and is involved in the activation of JNK after exposure to UV light (Zhang et al., 2002). JNK was also shown to be involved in the response to replication fork arrest and can stabilise p53 directly upon UV damage (Buschmann et al., 2001). DNA damage checkpoint pathways also show connections to the MAPK p38 stress pathway because, during G1 and intra-S checkpoints, p38 is able to activate the p53–p21 pathway and to inactivate Cdc25A. Moreover, p38 is important for establishment of the UV-induced G2 checkpoint by direct phosphorylation of Cdc25B and Cdc25C (Bulavin et al., 2001; Reinhardt et al., 2007).

Stress signalling induces reorganisation of cell structures, mainly inside the nucleus. Increasing amounts of data point to the nucleolus as a central element that coordinates the stress response. The nucleolus contains ribosomal DNA (rDNA) and the machineries required for the transcription of rDNA and its assembly in ribosomes. Nucleoli have three structural elements: fibrillar centres, dense fibrillar components (DFCs) and granular components. The nucleolar activity is highly regulated to adjust the ribosome synthesis rate to the cell's requirements, and RNA polymerase I inhibitors cause structural elements segregation (Al-Baker et al., 2004). Nucleolar transcription is regulated in response to DNA lesions in a p53- and ATM-dependent manner, and in response to ribotoxic or oxidative stress through the JNK pathway (Zhai and Comai, 2000; Mayer and Grummt, 2005; Kruhlak et al., 2007). Nucleoli are not only stress-signalling targets, but they are also proposed to be cell stress sensors that activate p53 by two different mechanisms. Disruption of the nucleoli structure by different stresses results in a block of MDM2–p53 transport from the nucleolus to the cytoplasm, which stabilises p53 (Rubbi and Milner, 2003). In addition, in response to stress, ARF p14 is released from disrupted nucleoli, which then binds MDM2, inducing p53 stabilisation (Lee et al., 2005).

Rad9B is a poorly characterised paralogue of Rad9A. Both Rad9A and Rad9B proteins show two PCNA-like domains and a weakly conserved C-terminal tail, which is heavily phosphorylated in Rad9A. Rad9B can form a complex with Rad1, Hus1, Rad17 and Rad9A (Dufault et al., 2003; Hopkins et al., 2003). Conditional deletion of Rad9A in mouse skin

showed an increase of Rad9B expression, suggesting a partial complementation between the two proteins (Hu et al., 2008). Recently, it was shown that targeted gene deletion of murine Rad9B produces severe developmental defects leading to embryonic death. *Rad9B*$^{-/-}$ embryonic stem cells were sensitive to DNA damage, but did not show any DNA damage checkpoint defect, suggesting that the Rad9B protein has a different function to Rad9A (Leloup et al., 2010).

Here, we studied the effects and localisation of Rad9B in human cells. We show that Rad9B can interact with components of the 9-1-1 complex and its overexpression delays cells in G1 phase of the cell cycle. Interestingly, Rad9B localises to nucleoli in the presence of DNA damage, suggesting a specific function for Rad9B linked to these nuclear domains.

Results

Rad9B interacts with Hus1, Rad17 and Rad1 but not with TopBP1

To gain insight into the biological function of Rad9B, we analysed which of the known Rad9A-interacting proteins can also bind Rad9B. For this, Rad9B was cloned into the pCI plasmid for expression of FLAG–Rad9B in U2OS cells and immunoprecipitated from untreated or UV-irradiated cells. FLAG–Rad9B could co-immunoprecipitate with Hus1, Rad1, Rad17 and the unphosphorylated form of Rad9A in both conditions, but not with PCNA (Fig. 1A). Rad9A has also been described to interact with TopBP1 (Lee et al., 2007), which we confirmed in our experiments. However, we were unable to detect an interaction between TopBP1 and Rad9B, indicating a different function for each of the two paralogues (Fig. 1B). A characteristic of the 9-1-1 complex is increased chromatin binding upon DNA damage in a Rad17–RFC-dependent manner (Bermudez et al., 2003). To study whether Rad9B could behave similarly, a subcellular fractionation of UV-treated cells expressing FLAG–Rad9B was performed. As described for Rad9A, FLAG–Rad9B can partially bind to the chromatin fraction even in unirradiated cells. However, its binding to the DNA did not significantly increase in the presence of damage (Fig. 1C).

Rad9B expression delays cells in G1 phase

Because Rad9B is related to PCNA, a study to test whether the protein has any role in replication was performed. First, we tried to colocalise FLAG–Rad9B with active replication forks detected by BrdU incorporation. Surprisingly, very few FLAG–Rad9B-positive cells were also positive for BrdU. By contrast, expression of FLAG–Rad9A did not affect BrdU incorporation (Fig. 2A). To test whether FLAG–Rad9B expression interferes with normal cell cycle progression, cells transfected with Rad9A or Rad9B stained for cyclin A, which is undetectable in G1, but shows moderate staining in S and peaks in G2 phase (Warmerdam et al., 2009). Interestingly, cells expressing FLAG–Rad9B showed a higher rate of cells without cyclin A staining, whereas FLAG–Rad9A expression did not modify the proportion of cyclin-A-positive cells when compared with untransfected cells (Fig. 2B). To determine whether the accumulation of G1 cells was reversible, cells collected at different times after transfection were analysed for cyclin A and Rad9B. The number of G2 cells increased (and accordingly the number of G1 cells decreased, data not shown) in Rad9B-expressing cells in the period from 48 to 60 hours after transfection (Fig. 2B, bottom right), suggesting that this is a reversible process. Moreover, cell cycle profiles of FLAG–Rad9B- or GFP-Rad9B-positive cells obtained by flow cytometry showed an increased G1 phase population, when compared with untransfected or empty-vector-transfected cells (Fig. 2C and Fig. 3A). Because GFP (compare GFP–spectrin to control in Fig. 3A) caused a small effect in the cell cycle profile, a similar assay was performed with an untagged version of Rad9B with similar results (Fig. 3A, right). Because G1 and early S phase cells are difficult to discriminate by flow cytometry, Rad9B-expressing cells were synchronised in early S phase using a thymidine block and the progression after thymidine release was analysed. GFP–Rad9B-expressing cells showed a normal S phase progression when compared with control cells, suggesting that expression of Rad9B does not interfere with S phase but with G1 phase progression (Fig. 3B).

Because Rad9B expression might trigger a DNA checkpoint arrest, we measured the levels of phosphorylated Chk1 and Chk2, γ-H2AX, p53 and p21 by western blot or immunofluorescence

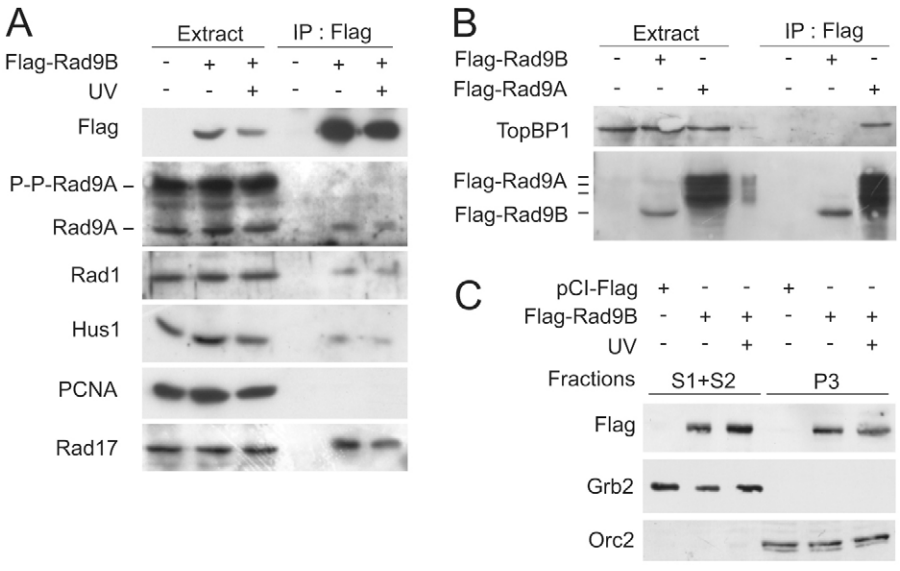

Fig. 1. Rad9B can interact with Rad1 and Hus1 but not with TopBP1. (**A**) U2OS cells expressing FLAG–Rad9B were UV irradiated (40 J/m^2) or left untreated. 1 hour after irradiation, immunoprecipitation with anti-FLAG beads was carried out before western blot analysis for the indicated proteins. (**B**) Cells were transfected with FLAG–Rad9A or FLAG–Rad9B. Immunoprecipitation and western blotting was performed as in A. (**C**) U2OS cells expressing FLAG–Rad9B were UV irradiated (40 J/m^2) or left untreated and 1 hour after irradiation were subjected to chromatin fractionation, to obtain a cytoplasmic soluble fraction (S1), nuclear soluble fraction (S2) and chromatin-enriched fraction (P3). Western blot analysis was carried out studying FLAG–Rad9B or using antibodies against Grb2 and Orc2 as markers for soluble and chromatin fractions, respectively.

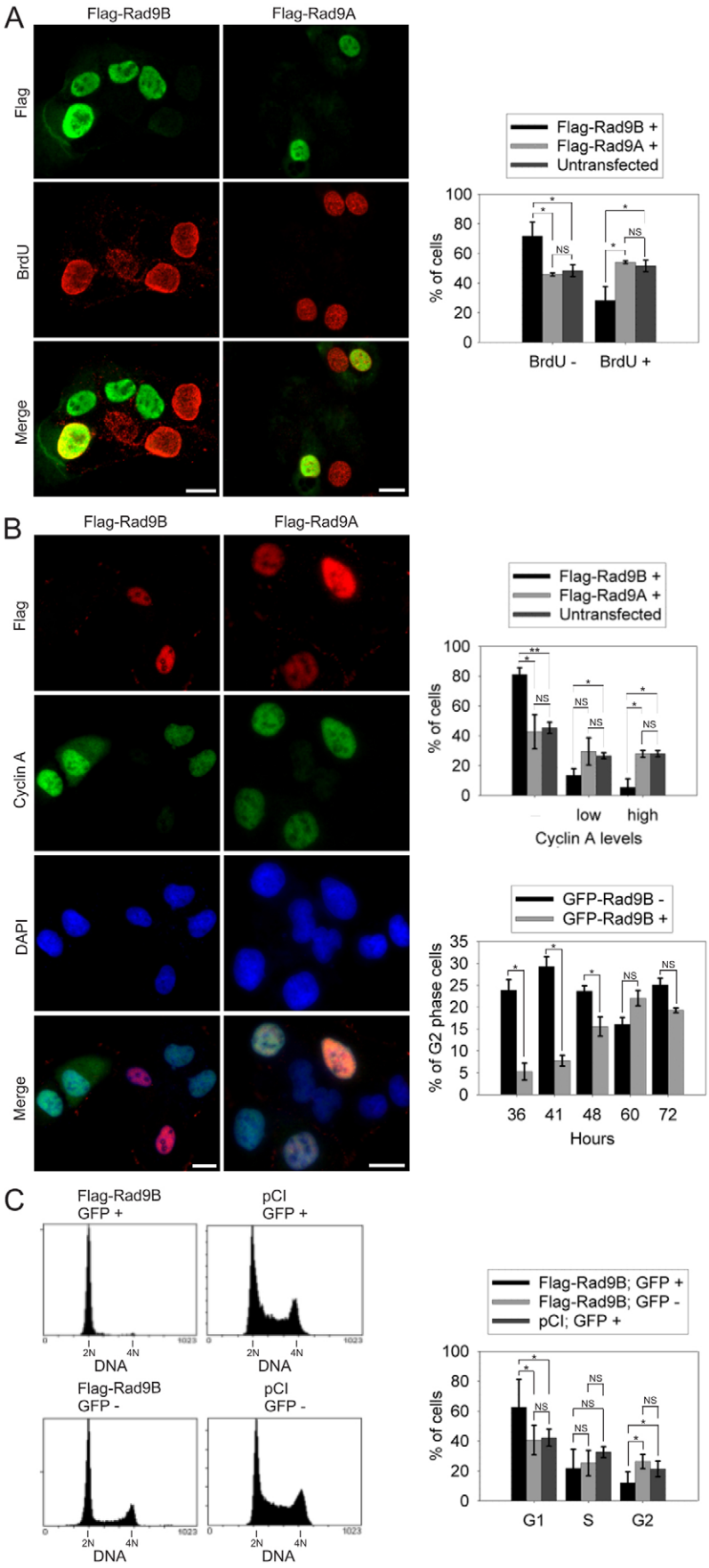

Fig. 2. Rad9B expression delays G1 progression. (**A**) U2OS cells expressing FLAG–Rad9B, FLAG–Rad9A or untransfected cells were synchronised at G1–S using thymidine for 24 hours. 5 hours after release, cells were incubated for 10 minutes with bromodeoxyuridine, fixed and subsequently subjected to immunofluorescence using antibodies against BrdU and FLAG. The percentage of FLAG-positive cells either positive or negative for BrdU were scored by analysing three independent experiments. The mean, s.d. and statistical significance are shown on the right. (**B**) U2OS cells expressing FLAG–Rad9B, FLAG–Rad9A or untransfected cells were stained for immunofluorescence using antibodies against FLAG and cyclin A. The percentage expression of Rad9B and Rad9A was analysed in cells with different expression levels of cyclin A (top right). The percentage of G2 phase cells (high levels of cyclin A) was also studied at different time points after transfection of GFP−Rad9B (bottom right). (**C**) U2OS cells co-transfected with vectors expressing FLAG–Rad9B and GFP–spectrin, or empty pCI–FLAG and GFP–spectrin were prepared for flow cytometry analysis using propidium iodide staining. The cell cycle profile of GFP positive (+) and GFP negative (-) cells is shown (left panel). Analysis of the percentage of cells in different stages of cell cycle from six experiments is shown. *$P<0.05$; **$P<0.001$. Scale bars: 20 μm.

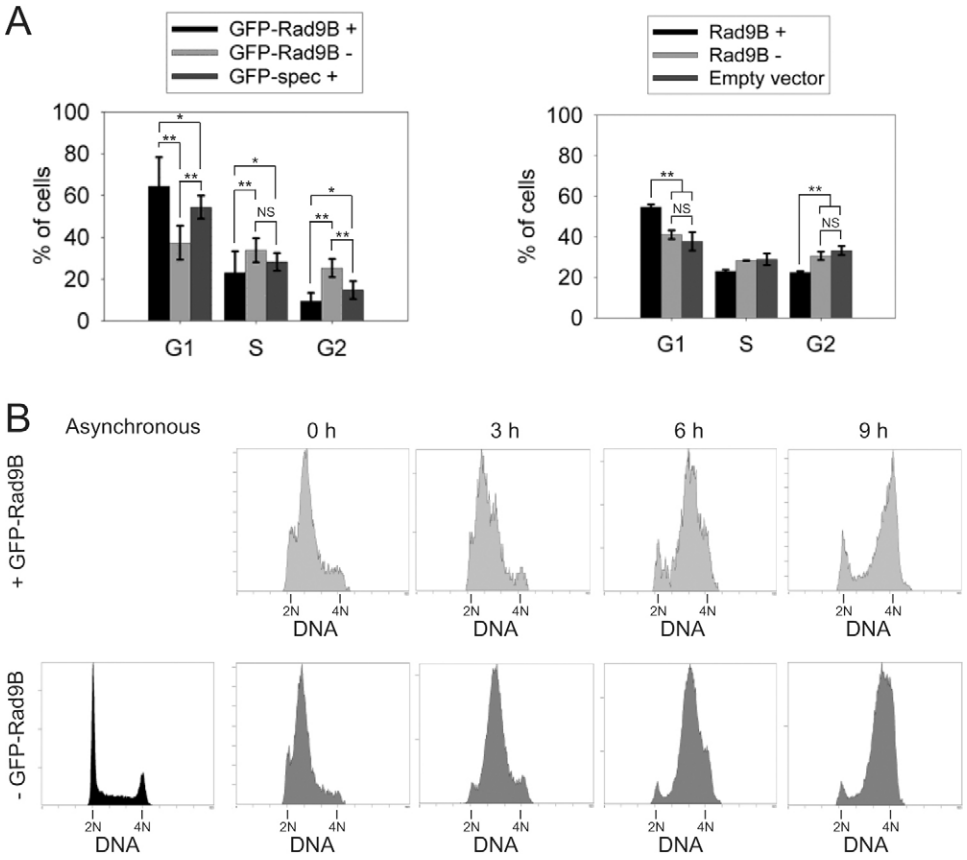

Fig. 3. Rad9B expression does not delay S phase progression. (**A**) U2OS cells were transfected with GFP-Rad9B or GFP-spectrin vectors, and then cell cycle profiles of GFP positive (+) or GFP negative (-) cells were measured and percentage of cells in the different stages of cell cycle from 12 experiments were scored (left). Right panel, as left, but with overexpressed untagged Rad9B and staining with antibody against Rad9B to distinguish Rad9B-positive cells. Percentages of cells in G1, S and G2 were calculated from three different experiments. Mean values, s.d. and statistical significance are shown. (**B**) U2OS cells were blocked at G1–S transition with thymidine for 24 hours, then transfected with GFP–Rad9B and 24 hours later thymidine was removed. Cells were collected at indicated time points after release and their cell cycle profiles were analysed by flow cytometry. $^{*}P<0.05$; $^{**}P<0.001$.

(supplementary material Fig. S1). None of these markers showed a change compared with the control condition, indicating that the activation of these pathways is not likely to be the cause of the G1 phase arrest by Rad9B. To completely dismiss the role of p53 in Rad9B-induced G1 arrest, we downregulated p53 levels in Rad9B-expressing cells. These cells show the same G1 arrest phenotype as control downregulated cells, thereby excluding a role for p53 in this G1 arrest (supplementary material Fig. S2).

Rad9B localises to nucleoli in response to nucleolar stress

Next, to study whether Rad9B could play a similar role in the DNA damage response to Rad9A, we studied its subcellular localisation by immunofluorescence in response to UV irradiation. In untreated cells, FLAG–Rad9B localised to the nuclei and was not present in nucleoli. However, after UV irradiation, FLAG–Rad9B translocated to the nucleoli, which looked disrupted, as shown by regions with different optic density visible by DIC microscopy (Fig. 4A). Indeed, these distinctive DIC-detected nucleolar domains correlated with localisation of B23 (a nucleolar protein involved in ribosome biogenesis and a previously described marker for nucleolar disruption) outside the nucleoli (Fig. 4B) (Rubbi and Milner, 2003). To eliminate possible artefacts of antibody staining (i.e. masking of the epitope in non-damaged cells and epitope exposition in damaged cells), similar experiments were carried out with cells expressing GFP–Rad9B (Fig. 4C). In contrast to localisation of Rad9B, FLAG–Rad9A remained outside nucleoli after UV treatment (Fig. 4A). Nucleolus structure and function are very sensitive to agents perturbing RNA-polymerase-I-dependent transcription, including UV, and under these conditions, nucleolar components disassemble and transcription stops (Rubbi and Milner, 2003). Using a RNA polymerase I in situ assay, we confirmed that the incorporation of BrUTP was inhibited after UV treatment (supplementary material Fig. S3). To examine to which nucleolar component FLAG–Rad9B localised, co-staining for FLAG–Rad9B and the structural elements, dense fibrillar centers (fibrillarin) or fibrillar centres (UBF) was performed by immunofluorescence. No colocalisation was detected of FLAG–Rad9B with any of these domains (Fig. 4D). A recent publication reported the accumulation of p21 in spherical structures that are formed in disrupted nucleoli and called INoBs (intranucleolar bodies) (Abella et al., 2010). To determine whether FLAG–Rad9B migrates to these structures, cells were treated with adriamycin and co-stained for p21 (Abella et al., 2010). Localisation of both proteins was observed inside the INoBs bodies, although a detailed analysis by confocal microscopy revealed that p21 and Rad9B co-compartmentalised, but did not co-localise inside these structures (Fig. 4E). Also, co-immunoprecipitation studies with overexpressed proteins indicated that Rad9B could interact with p21 in both basal conditions and under nucleolar stress (supplementary material Fig. S4A), and although relatively weak, the interaction was reproducible and might indicate a common function of the two proteins.

To investigate the migration of Rad9B to nucleoli in more detail, kinetic studies were carried out. The observed staining patterns were divided into three groups: (1) normal nucleoli and no Rad9B migration; (2) disrupted nucleoli without Rad9B; and (3) disrupted nucleoli containing Rad9B (FLAG or GFP tagged). At early time points after UV treatment (20–40 minutes), an

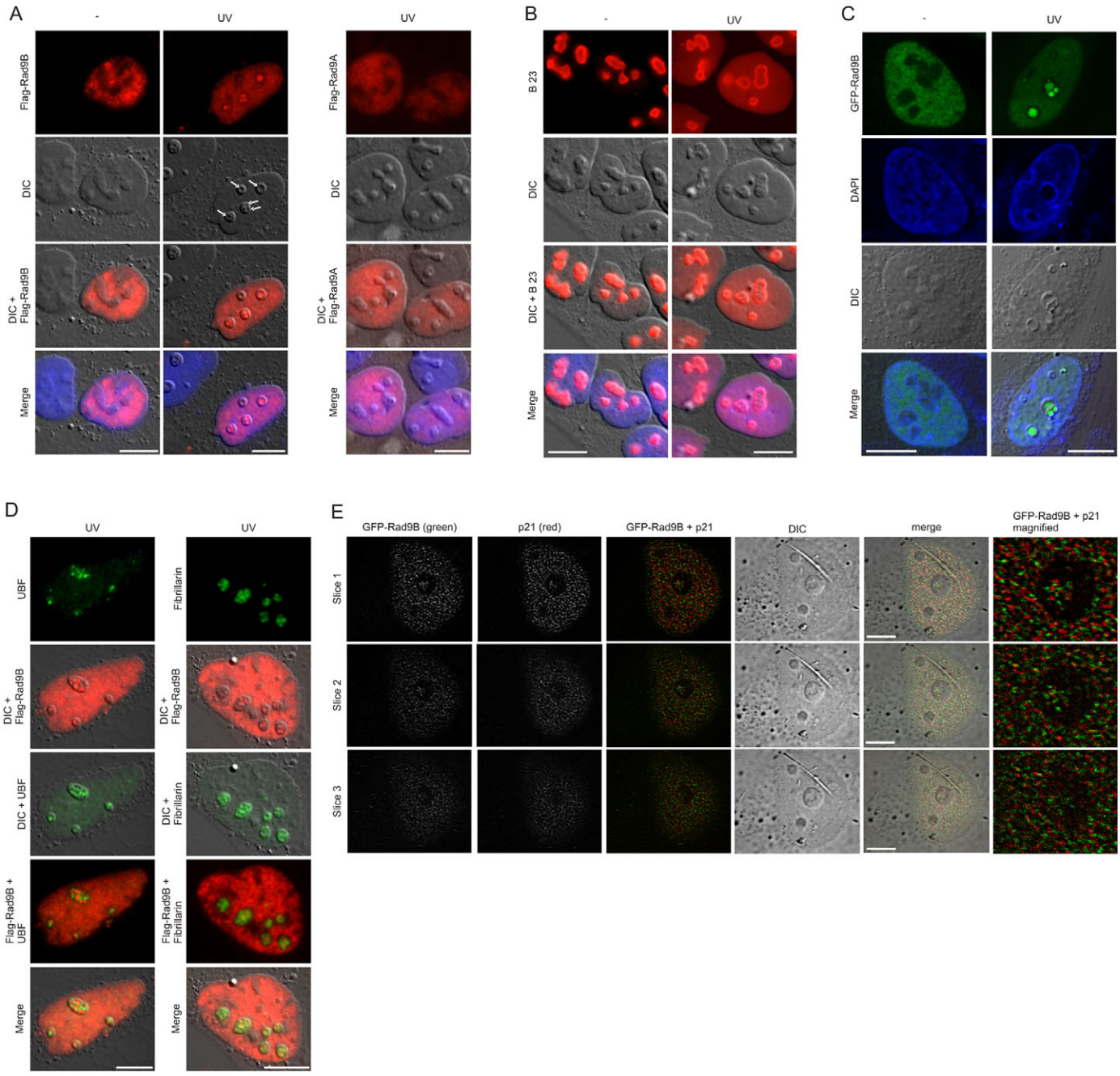

Fig. 4. Rad9B migrates to nucleoli after UV irradiation and colocalises with p21 in intranucleolar bodies. (**A**) U2OS cells expressing FLAG–Rad9B or FLAG–Rad9A were treated or not with UV (40 J/m^2) and fixed 1 hour after irradiation. Cells were subsequently analysed for FLAG immunofluorescence and by differential interference contrast microscopy (DIC). Arrows indicate disorganised nucleoli with Rad9B localisation. (**B**) U2OS cells treated with UV (40 J/m^2) immunostained for B23. (**C**) U2OS transfected with GFP-Rad9B, treated with UV (40 J/m^2). (**D**) U2OS cells transfected with FLAG–Rad9B, UV irradiated (40 J/m^2) and immunostained with the indicated antibodies. (**E**) Cells as in A, treated with adriamycin for 16 hours and co-stained with p21. Samples were analysed by confocal microscopy and deconvolution. Scale bars: 10 μm.

increase of cells in group 2 (disrupted –Rad9B) was observed, which decreased later, at or after 60 minutes, when more cells in group 3 (disrupted +Rad9B) were detected (Fig. 5A,B). These results suggest that UV causes a rapid nucleolar disassembly after which FLAG–Rad9B or GFP–Rad9B migrate to the disrupted nucleoli. To analyse whether Rad9B localisation into nucleoli specifically needed the irradiation inside the nucleoli or just the nucleoplasm, pore filters were used to irradiate cells and were analysed by immunofluorescence of XPB (xeroderma pigmentosum B) protein to identity the damaged area. As shown in Fig. 5C, the presence of DNA damage outside the nucleoli did not cause disruption of nucleoli, and/or the migration of FLAG–Rad9B. Quantification of this effect indicated that local irradiation outside the nucleoli did not produce nucleolar

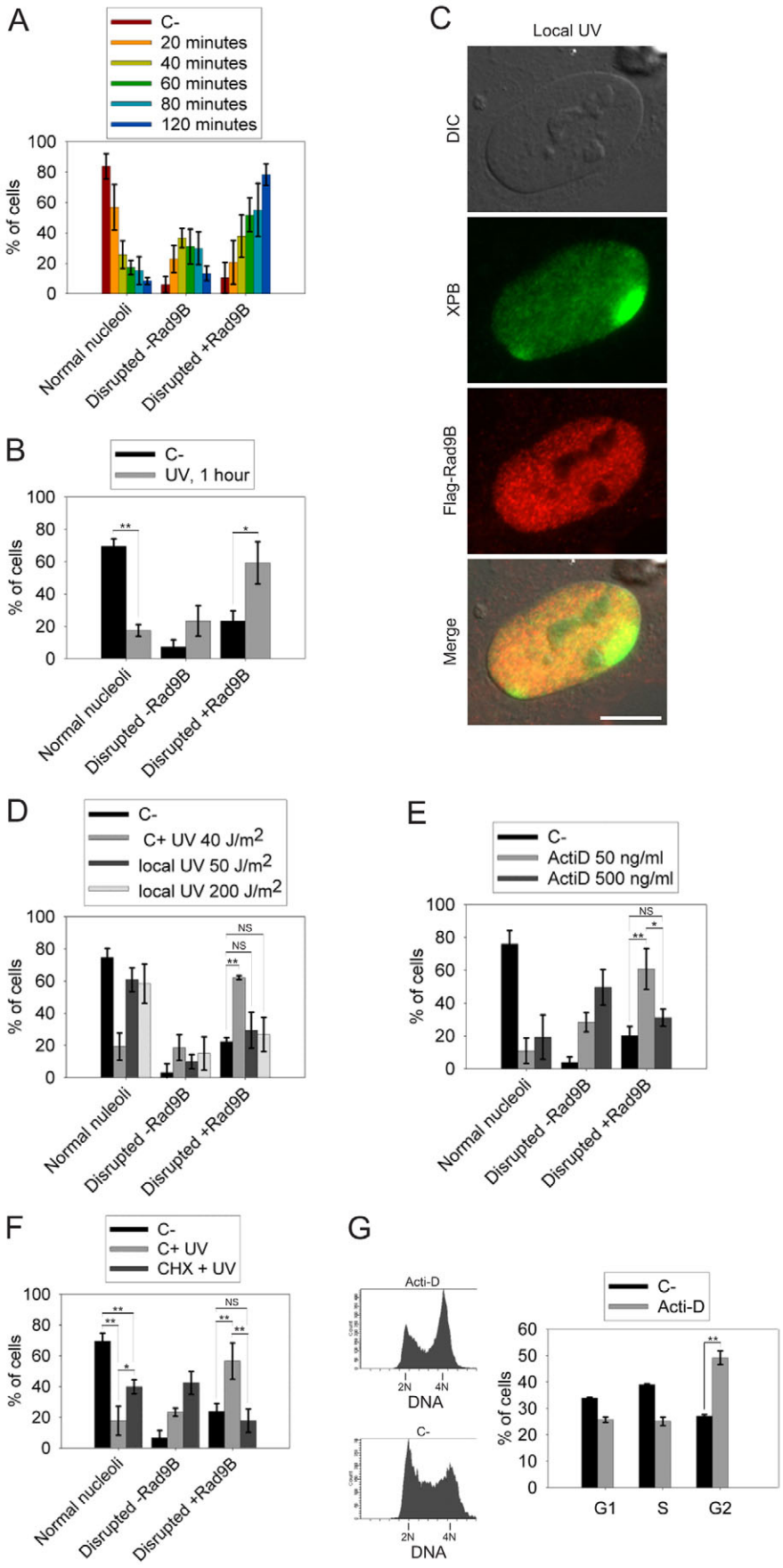

Fig. 5. Rad9B migrates to nucleoli after disruption of RNA polymerase I activity. (**A**) Cells expressing FLAG–Rad9B or (**B**) GFP–Rad9B were UV irradiated (40 J/m^2) or left untreated and fixed at the indicated times post treatment for immunostaining with anti-FLAG or analysed by direct fluorescence from GFP and DIC microscopy. Cells showing normal nucleoli, disrupted nucleoli and no FLAG/GFP-Rad9B or disrupted nucleoli with FLAG/GFP-Rad9B were scored from four experiments and percentages of cells in each category are represented. Error bars represent s.d. (**C**) U2OS cells expressing FLAG–Rad9B were locally UV irradiated (50 J/m^2) using polycarbonate filters (see the Materials and Methods for details). 1 hour later, cells were fixed and immunostained for XPB and FLAG before analysis. (**D**) Cells locally UV irradiated using indicated doses and control cells treated with UV (40 J/m^2) or not, were analysed for the presence of disrupted nucleoli and FLAG–Rad9B foci formation. The percentages of cells in each category are scored as in A. Histogram represents the analysis of three independent experiments with error bars representing s.d. (**E**) U2OS cells expressing FLAG–Rad9B treated with the indicated doses of actinomycin D for 1 hour and scored as in A. (**F**) U2OS cells expressing FLAG–Rad9B incubated with cycloheximide for 1 hour before UV irradiation (40 J/m^2). 1 hour after irradiation cells were fixed, analysed and scored as in A, together with positive control cells not incubated with the drug (C+ UV) and untreated cells (C-). (**G**) Cell cycle profiles of U2OS cells treated with 50 ng/ml of actinomycin D for 16 hours analysed by flow cytometry (left). Percentage of cells in the different stages of cell cycle from three different experiments was calculated. Mean values, s.d. and statistical significance are shown. *P<0.05; **P<0.001. Scale bar: 10 μm.

disruption, indicating that nucleoli need to be directly affected to become disorganised (Fig. 5D).

Because the main function of the nucleoli is to transcribe rRNA, we reasoned that the disorganisation of the nucleoli by UV might be caused by a direct effect on transcription, and therefore, any agent perturbing rRNA transcription might have the same effect as UV. To examine this, actinomycin D was used at low concentration to inhibit RNA polymerase I and high concentration to inhibit both RNA polymerase I and II. High and low concentrations of actinomycin D caused, as expected, disruption of nucleoli, but only the low concentration promoted the relocalisation of FLAG–Rad9B (Fig. 5E). Thus, we hypothesised that migration of Rad9B depended on RNA-polymerase-II-mediated transcription and protein synthesis. This was tested by incubation with the translation inhibitor cycloheximide before UV irradiation, after which Rad9B migration was measured. In these conditions, UV caused the disruption of nucleoli, but FLAG–Rad9B was not present (Fig. 5F). Moreover, we tested whether the inhibition of RNA polymerase I was related to the G1 arrest observed after Rad9B overexpression. FACS profiles showed that low concentrations of actinomycin D caused an increase of cells in G2–M phase, indicating that Rad9B expression and inhibition of RNA polymerase I have different effects on cell cycle progression (Fig. 5G). Taken together, these data indicate that perturbing transcription in nucleoli results in a disruption of the structure, thereby promoting migration of FLAG–Rad9B to nucleoli – a process that is dependent on RNA polymerase II.

To investigate which pathways are involved in Rad9B migration to nucleoli upon UV irradiation, cells were incubated with inhibitors against different cellular pathways that are activated upon UV irradiation, and then Rad9B migration and nucleolar disruption were studied. Interestingly, a p38 inhibitor and caffeine or wortmannin, or a combination of both, reduced the percentage of cells with FLAG–Rad9B in nucleoli, whereas the formation of disrupted nucleoli was not affected. However, inhibitors of ATM, DNA-PK and Chk1 did not affect Rad9B migration (Fig. 6A). To confirm the importance of ATR for Rad9B localisation to nucleoli, ATR protein levels were downregulated by siRNA. As expected, cells with low ATR levels were unable to signal Rad9B to disrupted nucleoli (Fig. 6B). To study whether Rad17 was required for Rad9B localisation to nucleoli, we downregulated Rad17 by shRNA and studied Rad9B subcellular localisation in the presence of UV. Surprisingly, lack of Rad17 did not affect Rad9B localisation to nucleoli (Fig. 6C). Because the 9-1-1 complex is involved in the activation of ATR, to further characterise the involvement of the ATR pathway in the molecular mechanism of Rad9B we analysed the size of elution of Rad9B and Hus1 in a gel filtration both in the presence and absence of actinomycin D. Surprisingly, Rad9B, unlike the described size of the 9-1-1 complex, eluted with high molecular mass, indicating that it forms a large complex (Fig. 6D). Interestingly, Hus1, Rad1 and the low migrating form of Rad9A predominantly co-elute with a size corresponding to the 9-1-1 complex (~260 kDa), but when Rad9B was expressed in the presence of actinomycin D, a significant amount of these proteins also co-eluted with Rad9B. This indicates that, Rad9B, the 9-1-1 complex and Rad17 might be part of a large complex upon treatment with actinomycin D (Fig. 6D).

Moreover, pretreating cells with a JNK inhibitor reduced the percentage of FLAG–Rad9B in disrupted nucleoli, suggesting an important role of the JNK-dependent stress pathway in this process (Fig. 7A). JNK becomes activated by osmotic stress or heat, and under these conditions, nucleoli appear to be intact in DIC images, but confocal 3D analysis showed that Rad9B localised to the nucleolar ends (Fig. 7B).

Disruption of nucleolar activity triggers the stabilisation of p53; however, nucleolar activity is also a target of p53 (Zhai and Comai, 2000; Pestov et al., 2001). Because UV exposure leads to stabilisation of p53, it is possible that p53 is involved in migration of Rad9B to nucleoli. To test this, the p53 pathway was activated using the Hdm2 antagonist Nutlin-3. Our results showed no difference between treated and control cells, and therefore indicate that activation of this pathway does not seem to be the only requirement for triggering nucleoli disruption or Rad9B migration to nucleoli (supplementary material Fig. S4B).

To investigate whether the expression of FLAG–Rad9B itself could affect transcription, a RNA polymerase I in situ assay was performed. FLAG–Rad9B expression did not change the activity of RNA polymerase I (supplementary material Fig. S5A).

Rad9B C-terminal tail is required for migration and localisation to nucleoli

We next tried to define the regions of Rad9B responsible for its migration to nucleoli. Because abrogation of ATR function affects Rad9B relocation, it was possible that ATR-mediated phosphorylation of Rad9B results in migration. ATR typically phosphorylates serine or threonine residues that are followed by glutamine. Therefore, serines or threonines with these characteristics were mutated to alanine in Rad9B (positions 139, 172 and 289) and the migration of the mutants was studied. A triple mutant (S3A) behaved similarly to the wild-type protein in nucleolar migration upon UV exposure, indicating that these positions do not influence Rad9B relocation, which makes it unlikely that ATR plays a direct role in this process (Fig. 8A). These results are in agreement with a lack of electrophoretic mobility change in response to nuclear stress (supplementary material Fig. S5B).

To map which domain(s) was involved in the migration to nucleoli, several deletions were made fused to FLAG and were tested for immunofluorescence analysis after UV treatment (Fig. 8B). Because fragments containing only the first PCNA-like domain (F1+ and F2) did not localise to the nucleus, we were not able to study their migration to the nucleoli. Interestingly though, F1+ fragment localised to mitochondria (supplementary material Fig. S6) and could be related to the function of the BH3 domain located at the N-terminus of the protein. Fragments including the second PCNA-like domain (F3 and F5) showed low migration rates, whereas a peptide containing only the C-terminal tail was unable to localise to nucleoli. However, when the C-terminal tail was deleted (F6+) the migration rate decreased compared with that of the full-length protein (Fig. 8C). These results suggest that all domains contribute to the nucleolar localisation, but some artefacts could have been introduced by misfolding of deletion mutants. Because Rad9A does not migrate to nucleoli after UV exposure (Fig. 8D), and to preserve the global folding of the protein, Rad9A–Rad9B chimeras were generated by interchanging their structural domains (Fig. 8E), and localisation to nucleoli after UV irradiation was studied. Interestingly, chimeras containing the C-terminal tail of Rad9B (Q3 and Q4) were able to localise to nucleoli after UV,

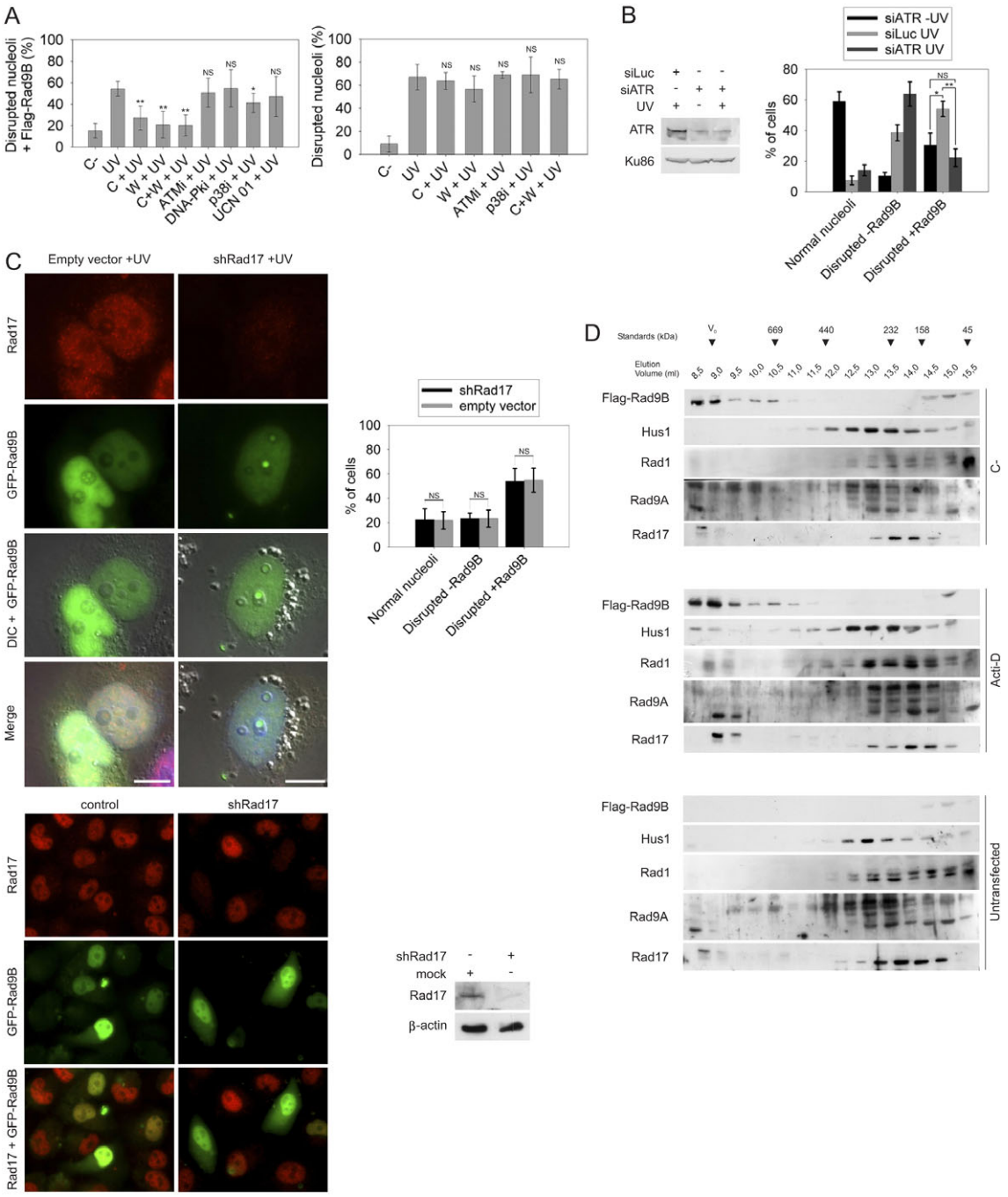

Fig. 6. Rad9B localisation in disrupted nucleoli depends on ATR signalling. (**A**) U2OS cells expressing FLAG–Rad9B pre-treated, where indicated, with caffeine (C), wortmannin (W), or both (C+W), the ATM inhibitor KU55933, the DNA-PK inhibitor NU7441, the p38 inhibitor SB203580, or the Chk1 inhibitor UCN-01 for 1 hour before UV treatment (40 J/m^2). 1 hour later, cells were analysed for Rad9B migration to disrupted nucleoli (left panel) and total number of disrupted nucleoli (right panel). The histograms show the means, s.d. and statistical significance from four independent experiments. (**B**) U2OS cells transfected with siRNA against ATR or luciferase as a control, twice in 72 hours. 24 hours after the first siRNA treatment, cells were also transfected with the FLAG–Rad9B expression vector. 48 hours later, cells were UV treated (40 J/m^2) when indicated and 1 hour later, analysed by western blot for the indicated antibodies (left panel) or by immunostaining for FLAG and scored as in Fig. 5A (right panel). Histogram represents the means and s.d. from three independent experiments. (**C**) U2OS cells transfected with shRNA against Rad17 and 24 hours later co-transfected with GFP–Rad9B and shRNA against Rad17. After an additional 36 hours, cells were UV treated (40 J/m^2) and finally fixed. Samples were then immunostained for Rad17 and analysed by fluorescence microscopy. Cells belonging to the different groups indicated were scored from three different experiments and percentages of cells and s.d. calculated (Top right panel). Bottom panels show the downregulation of Rad17 using shRNA against Rad17 in U2OS cells by immunofluorescence microscopy and in HEK293T cells by western blot. (**D**) U2OS cells transfected or not with FLAG–Rad9B were lysed and soluble fraction was loaded in a gel filtration assay. After elution, samples were precipitated with acetone, and after resuspension, analysed by western blot for the indicated proteins. Arrows indicate the peak of elution of different molecular mass standards. *$P<0.05$; **$P<0.001$. Scale bars: 10 μm.

whereas the C-terminal tail of Rad9A prevented the migration of PCNA-like domains of Rad9B (Q2, Fig. 8F). These results highlight the existence of a nucleolar targeting sequence in the Rad9B C-terminal tail that responds to nucleolar stress.

The regions of Rad9B that are important for the G1 phase arrest were mapped by overexpressing the different chimeras in U2OS cells and analysing the cell cycle phases by staining for cyclin A. Notably, expression of chimeras containing the C-terminal tail of Rad9B (Q3 and Q4) increased the rate of cells in G1, whereas expression of chimeras with the C-terminus from Rad9A, did not change the cell cycle distribution (Fig. 8G). We therefore conclude that the Rad9B C-terminal tail is important for both the migration to nucleoli and the cell cycle delay phenotype, and it is possible that both characteristics are linked.

Finally, to study whether migration of Rad9B was restricted to G1 cells, we analysed Rad9B localisation upon UV treatment at different stages of the cell cycle. In asynchronous populations, Rad9B was detected in disorganised nucleoli in S and G2 cells as judged by the co-staining with cyclin A (Fig. 8H). Additionally, cells were synchronised with thymidine at the moment of transfection and released for different times to obtain populations enriched in S and G2 phase cells. We detected Rad9B in nucleoli after UV treatment during these phases, which was similar to results in asynchronous cells (Fig. 8I), indicating that the migration to disrupted nucleoli is not restricted to G1 phase cells.

Discussion

Data presented here show a distinct in vivo behaviour for human Rad9B compared with its paralogue Rad9A. Rad9B is able to interact with Rad1, Hus1 and Rad17 and forms part of a large complex. However, Rad9B, unlike Rad9A, is not able to interact with TopBP1, which suggests a role of Rad9B unrelated to the activation of ATR. Moreover, in normal conditions, the overexpression of Rad9B causes a G1–S delay by a mechanism that is independent of p53, p21, Chk1, Chk2 or H2AX: an effect that differs from Rad9A function, which plays its major role during intra-S and G2 phase checkpoints. These two proteins also show different behaviour in response to DNA damage; Rad9B localises to a specific domain within disrupted nucleoli after UV irradiation or actinomycin D treatment, whereas only a small proportion of cells showed localisation of Rad9A to nucleoli and their number did not increase upon damage. Therefore, our data suggest that Rad9B is not involved in similar processes to Rad9A, but instead suggest a different role related to the nucleolar stress response.

The migration of Rad9B to nucleoli is observed after exposure to UV or actinomycin D, which are known to directly interfere with the physiology of the nucleolus and cause the disruption of its structure. Moreover, Rad9B migration and nucleolar disruption only depends on UV exposure inside nucleoli, because high doses of UV applied to the nucleoplasm did not affect nucleolar structure or cause Rad9B relocation.

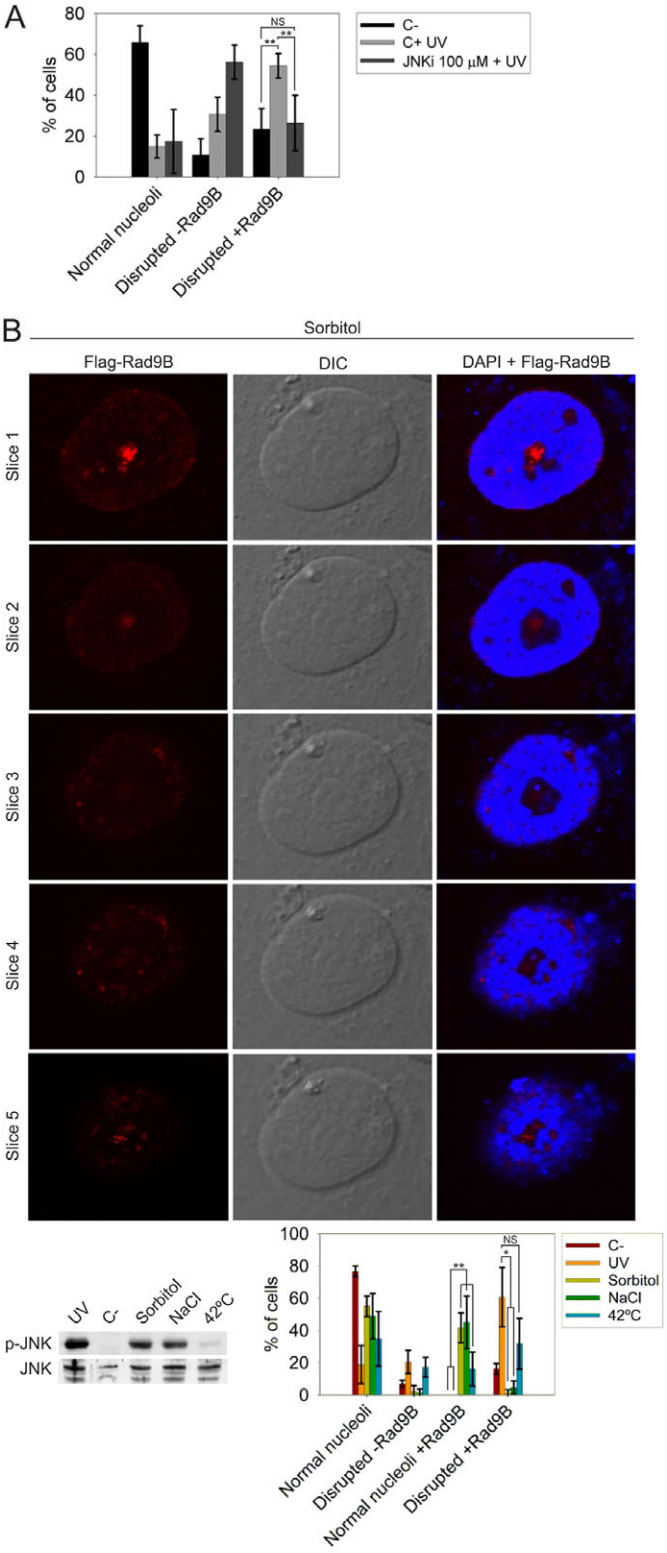

Fig. 7. Rad9B localisation in disrupted nucleoli depends on JNK signalling. (**A**) U2OS cells expressing FLAG–Rad9B were incubated with JNK inhibitor SP600125 for 1 hour or left untreated. Cells were then UV irradiated (40 J/m^2), and immunostained 1 hour post irradiation and scored as in Fig. 5A. Mean values and s.d. from six experiments are shown. (**B**) U2OS cells were transfected with FLAG–Rad9B plasmid and incubated with sorbitol for 30 minutes and immunofluorescence analysis of FLAG and DIC was performed (top panel shows different confocal *Z*-sections of a cell with Rad9B migration to normal nucleoli). Transfected U2OS cells were incubated with sorbitol or NaCl for 30 minutes or at 42℃ for 1 hour and were lysed and analysed by western blot against the indicated antibodies (bottom left panel) or stained for FLAG, analysed by fluorescence microscopy and DIC and scored as described in Fig. 5A (bottom right panel). Mean values and s.d. were calculated from three independent experiments. *P<0.05; **P<0.001.

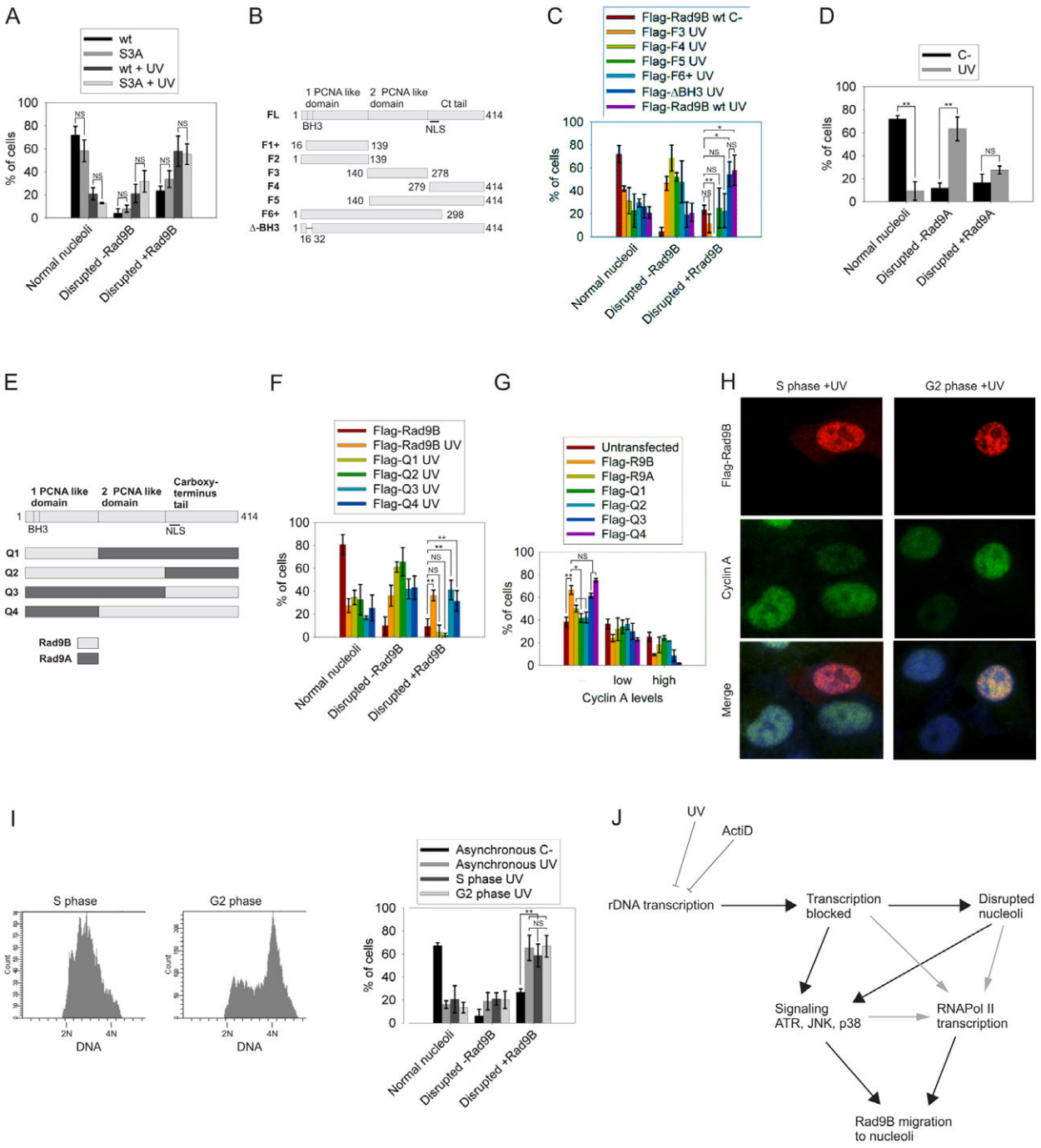

Fig. 8. Rad9B C-terminus is crucial for nucleolar localisation and the G1 delay. (**A**) FLAG–Rad9B wild type or S3A mutant was expressed in U2OS cells; cells were UV irradiated (40 J/m^2) and 1 hour later, stained for FLAG and analysed as described in Fig. 5A. Statistical analysis from three experiments is shown. (**B**) Schematic overview of Rad9B domain, motifs and the different deletion mutants. (**C**) U2OS cells expressing the indicated Rad9B truncations fused to FLAG, were transfected, stained and scored as in Fig. 5A. Data obtained from the analysis of three experiments are presented. (**D**) U2OS cells expressing FLAG–Rad9A were UV irradiated, analysed and scored from three independent experiments as described in Fig. 5A. (**E**) Schematic representation of the different chimeras obtained by fusing the indicated domains of Rad9B and Rad9A. (**F**) Staining and analysis of migration to nucleoli of the indicated chimeras after UV treatment, as described for Fig. 5A. The histogram represents five independent experiments. (**G**) U2OS cells transfected with the indicated constructs were fixed and stained for FLAG and cyclin A, analysed and scored as in Fig. 2B. Histogram shows the percentage of cells with undetectable, low or high levels of cyclin A, from two independent experiments. (**H**) Asynchronous U20S cells transfected with FLAG–Rad9B were analysed using immunofluorescence against cyclin A and FLAG after UV treatment as described in Fig 5A. Shown are examples of transfected cells with positive migration to nucleoli in S and G2 stages of cell cycle, as judged by cyclin A staining. (**I**) U2OS cells were transfected with GFP–Rad9B in the presence of thymidine and released 36 hours post transfection for 3 and 10 hours to obtain populations enriched in S phase and G2 phase, confirmed by flow cytometry analysis of the Rad9B–GFP-positive cells (left panels). On the right, analysis of the migration of Rad9B–GFP to nucleoli in the presence of UV is shown in synchronised S and G2 cells compared with an asynchronous population. Three independent experiments were used for the statistical analysis. (**J**) A model for Rad9B migration to nucleoli. Grey arrows indicate possible regulatory mechanism of RNA Pol II transcription. *P<0.05; **P<0.001.

Interestingly, migration of Rad9B to the nucleoli is dependent on several signalling pathways. We have shown that ATR, but not Chk1, is necessary for Rad9B relocalisation. ATR kinase is involved in the DNA damage response, mainly in response to single-stranded lesions or replication fork problems (Yang et al., 2003). Upon occurrence of these lesions, ATR kinase activity is stimulated and ATR binds DNA, in an RPA- and ATRIP-dependent manner (Unsal-Kacmaz et al., 2002). ATR and RPA have also been directly related to a cellular response that triggers the stabilisation of p53 upon RNA polymerase II transcription inhibition by UV or actinomycin D treatment (Derheimer et al., 2007). Moreover, in the presence of DNA damage, ATR and Rad9A are more efficiently recruited to transcriptionally active genome areas than to untranscribed areas, and a model has been proposed in which blocked transcription forks sense DNA damage to trigger a DNA damage response (Jiang and Sancar, 2006). The data presented here are compatible with a model in which transcriptional stress in the nucleoli triggers an ATR-dependent response that results in Rad9B recruitment to the nucleoli (Fig. 8J). How ATR triggers Rad9B migration is a point of further investigation. ATR does not seem to phosphorylate Rad9B directly because Rad9B with all SQ or TQ motifs mutated showed a similar behaviour to the wild-type protein.

Our experiments indicate that the stress kinase JNK is also important for Rad9B migration to stressed nucleoli (Fig. 8J). This pathway is activated in response to different stresses including heat and osmotic shock or irradiation (Davis, 2000; Martindale and Holbrook, 2002). JNK phosphorylates TIF-IA, an essential transcription factor of the RNA polymerase I machinery, resulting in its release from nucleoli and a block of rRNA synthesis (Mayer and Grummt, 2005). Also, release of p14ARF and B23 from the nucleoli is a JNK-dependent process (Yogev et al., 2008). Here, we describe the localisation of Rad9B to disrupted nucleoli after UV and actinomycin D treatment, but also to normal nucleoli in response to osmotic shock and heat, suggesting a function for Rad9B related to nucleoli and the JNK pathway. We also show that the activation of this stress response, including the migration of Rad9B into nucleoli, requires RNA-polymerase-II-dependent transcription. This could be explained by the need for newly transcribed genes or the active transcription of genes whose proteins display short half-lives for this response. Because Rad9B migrates very quickly to the nucleoli after the inhibition of RNA polymerase I, we favour the possibility that proteins with short half-lives are actively involved in this process. Moreover, because ATR and JNK are stable proteins, our data suggest the involvement of mediator proteins responsible for the migration of Rad9B to disorganised nucleoli.

The migration of Rad9B to nucleoli is peculiar, because very few proteins are described to accumulate to nucleoli as a consequence of nucleolar stress (Guo et al., 2008; Banski et al., 2010) and most of the proteins described to localise to nucleoli are constitutively binding to nucleolar components or contain a nucleolar localisation sequence (Scott et al., 2001; Korgaonkar et al., 2005; Wang et al., 2011). Moreover, Rad9B localises to specific regions within nucleoli upon disruption of their structure, rather than throughout the nucleolus. To our knowledge, the only protein described to localise in such regions is p21 (Abella et al., 2010). Although not strong, we were able to detect an interaction between Rad9B and p21 in normal conditions, which could reflect a common role linked to the nucleoli. Among the few proteins that migrate to nucleoli upon stress, some, such as RNA helicase A or p21, localise to nucleoli as a result of inhibition of their export to the nucleoplasm or cytoplasm (Liu et al., 2007; Abella et al., 2010), and others such as RelA or p53 accumulate at the nucleoli by active signalling (Thoms et al., 2007; Karni-Schmidt et al., 2008), which inhibits the function of these proteins. Our data demonstrate that the C-terminus of Rad9B is important for the recruitment to nucleoli in an ATR- and JNK-dependent manner. Moreover, because the G1 phase delay caused by Rad9B overexpression also depends on the C-terminus tail of the protein, we suggest that migration to disrupted nucleoli and the G1 arrest might be functionally related. Very few proteins are described to actively migrate to nucleoli in response to stress and perform a new cellular function once they are relocated. Heat shock protein hsp70 was described to transiently migrate to nucleoli after heat shock and proposed to contribute to restore nucleolar morphology (Banski et al., 2010). Also, the tumour suppressor protein ING1 accumulates after UV irradiation to nucleoli and sensitises cells to apoptosis in those conditions. However, mutant ING1 proteins that are not targeted to nucleoli are not able to induce apoptosis after UV irradiation (Scott et al., 2001).

Recently, Rad9B heterozygous and knockout mice were reported (Leloup et al., 2010). Although the *Rad9B*$^{-/-}$ mice were not viable, heterozygous mice show developmental abnormalities. Furthermore, although knockout ES cells display higher sensitivity to gamma radiation and mitomycin C, they do not show DNA damage checkpoint defects. These data suggest that Rad9B does not play a role in DNA damage checkpoint regulation, which is in agreement with our results, but is rather required in some stages during development. This could explain why we failed to detect endogenous Rad9B by western blot in tumour cell lines (data not shown) and therefore we propose that Rad9B is exclusively expressed in certain tissues, or that protein expression is induced under certain conditions.

Nevertheless, our overexpression studies suggest a model in which the Rad9B responds to nucleolar stress after the activation of JNK-dependent stress signalling and ATR-dependent DNA damage response pathways, and actively accumulates within nucleoli, where it does not cause a transcription block. We speculate that Rad9B might contribute to the repair of the sites of (ribosomal) DNA lesions and it would be, therefore, possible that the function of Rad9B could be related to the maintenance of genomic stability at rDNA.

Materials and Methods

Cell culture, plasmids and transfections

U2OS and HEK293T cells were cultured in DMEM (Lonza) supplemented with 10% fetal bovine serum, 150 U/ml of penicillin and 150 μg/ml of streptomycin. When indicated, cells were irradiated with UV-C after washing with PBS. For local UV irradiation, coverslips were covered with 5 μm-pore-diameter polycarbonate filters (Millipore) before irradiation. Where indicated, cells were incubated with 10 mM caffeine (Sigma), 100 μM wortmannin (LC laboratories), 5 μM of DNA-PK inhibitor NU7441 (AstraZeneca), 10 μM of ATM inhibitor KU55933 (AstraZeneca), 5 μM of p38 inhibitor SB203580 (Sigma), 300 nM of Chk1 inhibitor UCN-01 (Sigma) or 100 μM of JNK inhibitor SP600125 (Sigma) 1 hour before UV irradiation, or 10 μg/ml of cycloheximide 2 hours before UV irradiation. In some experiments, cells were incubated with 50 or 500 ng/ml of actinomycin D (Applichem) for 1 hour, with 0.15 μg/ml of adriamycin for 16 hours, 100 nM mitotracker (Molecular Probes) for 15 minutes, 2 mM thymidine (Sigma) for 24 hours, 10 μM BrdU (Sigma) for 10 minutes, or 10 μM nutlin-3 (Sigma) for 9 or 33 hours. Where indicated, cells were incubated with 500 mM sorbitol or 300 mM NaCl for 30 minutes at 37℃, or at 42℃ for 1 hour.

Human *RAD9B* cDNA plasmid was kindly provided by Larry Karnitz (Mayo Clinic, Rochester, MN). Plasmid expressing GFP–p21 was a gift from Neus Agell (Universitat de Barcelona, Barcelona, Spain). Full-length or the indicated fragments of the *RAD9B* cDNA or full-length *RAD9B* were amplified by PCR and cloned in a modified pCI vector (Promega) to obtain N-terminally FLAG-tagged proteins or in pEGFP-C1 (Clontech) to obtain GFP fusions. *RAD9B* cDNA was also cloned in pET-28 bacterial expression vector (Novagen) and in pCI neo vector (Promega) to express a non-tagged version of *RAD9B* in human cells. Fragment Δ-BH3 was cloned in both vectors by obtaining a PCR fragment with an internal deletion corresponding to positions 17 to 31 using two sets of primers: 5′-GTCTAGTCTAGATATGGCAGCCATGCTGAAGTG-3′, 5′-GAAAAGGAAA-AGCGGCCGCTTAGAATATAGAGAAACTGCCATT-3′, 5′-AGGTGAAAGT-ATTTGGGAAACCATCTAAAAAAGGTCTTGC-3′ and 5′-CAAGACCTTTT-TTAGATGGTTTCCCAAATACTTTCACCT-3′.

FLAG–Rad9B with mutated Ser139, Ser172 and Ser289 to alanine was obtained by sited directed mutagenesis using the QuikChange Site-Directed Mutagenesis Kit (Stratagene) using the following primers: S139A (5′-ATAATATAT-GTTTTCAAGAAGCTCAGCCTTTGCAAGTTATT-3′ and 5′-AATAACTTGC-AAAGGCTGAGCTTCTTGAAAACATATATTAT-3′); S172A (5′-CATTGTTC-TTTTTACATCAGCTCAAGAGGAAGTTACTCTTG-3′ and 5′-CAAGAGTAA-CTTCCTCTTGAGCTGATGTAAAAAGAACAATG-3′); and S289A (5′-TC-ACCACAGTCACTGTGTCTTGCTCAGAAACGAAAAAGGTCAG-3′ and 5′-CTGACCTTTTTCGTTTCTGAGCAAGACACAGTGACTGTGGTGA-3′).

Chimeras were designed by fusing Rad9B and Rad9A domains. Chimera 1 (Q1) is composed of positions 1–139 from Rad9B and 130–390 from Rad9A and was cloned using the following primers: 5′-AATATATGTTTTCAAGAAAGTG-AGTCCCTGCAGGCCGTCTTC-3′ and 5′-GAAGACGGCCTGCAGGGACTC-ACTTTCTTGAAAACATATATT-3′. Chimera 2 (Q2): positions 1–278 from Rad9B and 273–390 from Rad9A, primers: 5′-AGAGCATCTTCACCACA-GTCACAGGACCTGGGCTCCCCAGAG-3′ and 5′-CTCTGGGGAGCCCAGG-TCCTGTGACTGTGGTGAAGATGCTCT-3′. Chimera 3 (Q3): positions 1–272 from Rad9A and 279–414 from Rad9B, primers: 5′-TCAGACACCGA-CTCGCACTCCAGAGCATCTTCACCACAGTCA-3′ and 5′-TGACTGTGG-TGAAGATGCTCTGGAGTGCGAGTCGGTGTCTGA-3′. Chimera 4 (Q4): positions 1–129 from Rad9A and 140–414 from Rad9B, primers: 5′-AACCTGTCCTTCCAGGACTGTCAGCCTTTGCAAGTTATTTTT-3′ and 5′-AAAAATAACTTGCAAAGGCTGACAGTCCTGGAAGGACAGGTT-3′.

To obtain an shRNA against Rad17, the following primers were cloned in pSuper: 5′-GATCCCCAGATGATTTCAAGGGGATGTTCAAGAGACATCCC-CTTGAAATCATCTTTTTTGGAAA-3′ and 5′-AGCTTTTCCAAAAAAGATG-ATTTCAAGGGGATGTCTCTTGAACATCCCCTTGAAATCATCTGGG-3′.

Plasmids were transfected with the standard calcium phosphate precipitate method or with lipofectamine 2000 (Invitrogen) and unless indicated, cells were collected for analysis 36 hours after transfection. siRNAs were transfected by using oligofectamine (Invitrogen) following the manufacturer's instructions. The following siRNA oligos were used: ATR, CCUCCGUGAUGUUGCUUGA (Thermo); Luciferase, CGUACGCGGAAUACUUCGA (Thermo); p53, AACUA-CUUCCUGAAAACAACG (Sigma).

Immunoprecipitation, cell fractionation and gel filtration

Cells subjected to immunoprecipitation were lysed for 15 minutes on ice in Buffer 1: 50 mM Tris-HCl, pH 8, 150 mM NaCl, 5 mM EDTA (pH 8), 0.5% NP-40, 1 mM NaF, 1 mM Na_3VO_4, 10 mM β-glycerolate and protease inhibitors (Complete, Roche). The extracts were centrifuged at 12,000 ***g*** for 10 minutes and then incubated with 10 μl of anti-FLAG-agarose gel (Sigma) for 3 hours at 4℃, on a wheel rotator, before washing three times with Buffer 1.

Cellular fractionation was performed as described previously (Mendez and Stillman, 2000). Cells were washed in PBS before being resuspended in 250 μl of cold Buffer A: 10 mM HEPES, pH 7.9, 10 mM KCl, 1.5 mM $MgCl_2$, 0.34 M sucrose, 10% glycerol, 1 mM DTT, 10 mM NaF, 1 mM Na_3VO_4 and protease inhibitors (Complete, Roche). They were then lysed on ice for 15 minutes by addition of Triton X-100 up to a 0.1% final concentration, and centrifuged to collect nuclei (4 minutes, 4℃, 1300 ***g***) and soluble cytoplasmic fraction as supernatant (S1). Nuclei were washed with Buffer A and lysed on ice for 5 minutes with 250 μl cold Buffer B: 3 mM EDTA, 0.2 mM EGTA, 1 mM DTT, 10 mM NaF, 1 mM Na_3VO_4 and protease inhibitors. Then, chromatin fraction was collected by centrifugation (4 minutes, 4℃, 1700 ***g***) and the soluble nuclear fraction (S2) was obtained as the supernatant. The final chromatin pellet (P3) was washed with Buffer B and pelleted by centrifugation (1 minute, 4℃, 10,000 ***g***).

Where indicated, the S1+S2 fraction described above was subjected to size exclusion chromatography using an AKTA FPLC workstation with a Superdex 200 10/300 GL column (GE Healthcare) at 4℃. Collected fractions were precipitated with acetone at –20℃. As molecular weight standards, the elution volumes of the proteins included in the HMG calibration kit (GE Healthcare) and BSA (Sigma) were measured. The void volume was measured using Blue Dextran 2000.

Antibodies for western blot and flow cytometry analysis

Primary antibodies against FLAG (M2, Sigma), Rad9A (Toueille et al., 2004), Rad1 and Hus1 (Francia et al., 2006), PCNA (PC10, SCBT), Rad17 (H-300, SCBT), TopBP1 (Rendtlew Danielsen et al., 2009), GFP, Orc2 (BD Pharma), ATR (N-19, SCBT), Ku86 (C-20, SCBT), Grb2 (BD Transduction), p53 (DO-1, SCBT), p21 (F-5, SCBT), β-actin (Sigma), phosphorylated SAPK/JNK (Thr183/Tyr185) and total SAPK/JNK (Cell Signaling) were used. HRP secondary antibodies were purchased from Jackson Immunoresearch. An anti-rabbit polyclonal Rad9B antibody was raised against recombinant His-tagged full-length human Rad9B by expressing the protein in *E. coli* and purifying it using Ni-NTA resin (Qiagen) following the manufacturer's instructions.

Immunofluorescence analysis and image acquisition

For immunofluorescence analysis, cells grown on coverslips were washed twice with PBS before fixation with 2% formaldehyde in PBS for 10 minutes at room temperature. Then, cells were washed with PBS and permeabilised with 0.5% NP-40 in PBS for 10 minutes and subsequently blocked with 5% BSA in PBS for 30 minutes. Cells were then incubated for different times with primary antibodies diluted in blocking solution with antibodies against: FLAG (M2, Sigma) for 30 minutes; fibrillarin (H-140, SCBT), UBF (H-300, SCBT), phosphorylated Chk1(Ser317) and phosphorylated Chk2(Thr68) (Cell Signaling), γ-H2AX (JBW301, Millipore) for 2 hours; p21 (F-5, SCBT), p53 (DO-1, SCBT), Rad17 (H-300, SCBT) for 1 hour; BrdU (BMC9318, Roche) for 4 hours; XPB (S-19, SCBT) for 3 hours; and cyclin A (H-432, SCBT) for 16 hours at 4℃. When needed, cells were washed and incubated with a second primary antibody. Then cells were washed and incubated with secondary antibodies in blocking solution: anti-rabbit Alexa Fluor 488 and/or anti-mouse Alexa Fluor 568 (Invitrogen) were applied for 50 minutes. After washing, coverslips were mounted using Slow-fade medium containing DAPI (Invitrogen). For statistical analysis preparations were randomly photographed using an Observer Z1 fluorescence microscope (Zeiss). 50 to 60 cells were analysed for each sample of each experiment and classified in each category. These data were transformed into percentages and mean values were compared using the Student's *t*-test (SPSS). For detailed analysis, images were acquired with an Olympus Fluoview FV1000 confocal microscope. Deconvolution microscopy was performed on the confocal microscope and a Metamorph Restoration Microscopy System (Molecular Devices). A *Z*-series of focal planes were digitally imaged and deconvolved with the Metamorph constrained iterative algorithm. This process removes out-of-focus light and reassigns it to its point of origin to generate high-resolution images. Multiple images containing several cells were collected and representative cells are shown. Images shown are deconvolved and represent single *Z*-sections.

RNA polymerase I assay

RNA polymerase I assay was performed as described previously (Wansink et al., 1993). Cells grown on coverslips were washed with TBS buffer (150 mM NaCl, 10 mM Tris-HCl, pH 7.4, 5 mM $MgCl_2$) and washed with glycerol buffer (20 mM Tris-HCl, pH 7.4, 5 mM $MgCl_2$, 25% glycerol, 0.5 mM PMSF, 0.5 mM EGTA). Cells were then mildly permeabilised with glycerol buffer supplemented with 0.05% Triton X-100 for 3 minutes. This buffer was replaced with transcription buffer: 100 mM KCl, 50 mM Tris-HCl, pH 7.4, 5 mM $MgCl_2$, 0.5 mM EGTA, 25% glycerol, 25 μM S-adenosyl-L-methionine (Sigma), 5 U/ml RNase inhibitor (RNasin, Promega), 1 mM PMSF, 0.5 mM of each nucleotide rATP, rCTP, rGTP (Promega), 0.2 mM BrUTP (Sigma) and 1 μg/ml α-amanitin (Sigma). The transcription reaction was performed for 15 minutes. Then, samples were washed twice with TBS buffer including 5 U/ml of RNasin, and immediately fixed with 4% formaldehyde in PBS. Samples were then immunostained following the procedure described above with the anti-BrdU antibody.

Labelling of mitochondria

For double labelling of mitochondria and F1+ FLAG-labelled fragment, cells were incubated with 100 nM of Mito Tracker (Molecular Probes) for 10 minutes just before fixation and subjected to immunofluorescence with antibodies against FLAG following the method described above.

Cell cycle analysis by flow cytometry

U2OS cells were cotransfected with FLAG–Rad9B and GFP–spectrin, or empty vector pCI and GFP–spectrin as a control. 36 hours later they were fixed with cold (4℃) 70% ethanol for 30 minutes on ice before incubation for 30 minutes at 37℃, with staining solution (0.1% Tween-20, 20 μg/ml propidium iodide, 40 μg/ml RNase, in PBS all reagents from Sigma). Cells were analysed using an Epics XL·MCL cytometer (Beckman Coulter) using a protocol to discriminate GFP-positive cells. Percentage of cells in each cell cycle phase was obtained from profiles and mean values were compared using the Student's *t*-test (SPSS). Cells transfected with GFP–Rad9B, or GFP–spectrin as a control, were analysed following the same protocol. To analyse DNA content of non-tagged Rad9B-positive cells, cells were fixed as described above and incubated with antibody against Rad9B in PBS containing 5% BSA for 1 hour at room temperature,

followed by an incubation with an anti-rabbit antibody coupled to Alexa Fluor 488 for 1 hour at room temperature. A final step of incubation with staining solution was performed before analysis, as described above. To synchronise cells expressing GFP–Rad9B in S-phase, U2OS cells were first blocked in early S-phase by incubation with 2 mM thymidine for 24 hours, then were transfected with Rad9–GFP expression vector for 24 hours before removing thymidine to allow progression through the cell cycle and collecting cells 3, 6, 9 hours after release.

Acknowledgements

The authors are grateful to V. Smits for careful reading of the manuscript.

Funding

This work was supported by grants from the Spanish Ministry of Science and Innovation [grant numbers SAF2010-22126; CONSOLIDER-Ingenio 2010 CDS2007-0015, FUNCIS (PI27/062)]. R.F. is supported by Instituto de Salud Carlos III. A.J.P.C. has a fellowship from Dirección General de Universidades e Investigación del Gobierno de Canarias, Spain, co-financed by the European Social Fund.

Supplementary material available online at
http://jcs.biologists.org/lookup/suppl/doi:10.1242/jcs.091124/-/DC1

References

Abella, N., Brun, S., Calvo, M., Tapia, O., Weber, J. D., Berciano, M. T., Lafarga, M., Bachs, O. and Agell, N. (2010). Nucleolar disruption ensures nuclear accumulation of p21 upon DNA damage. *Traffic* **11**, 743-755.

Al-Baker, E. A., Boyle, J., Harry, R. and Kill, I. R. (2004). A p53-independent pathway regulates nucleolar segregation and antigen translocation in response to DNA damage induced by UV irradiation. *Exp. Cell Res.* **292**, 179-186.

Banski, P., Mahboubi, H., Kodiha, M., Shrivastava, S., Kanagaratham, C. and Stochaj, U. (2010). Nucleolar targeting of the chaperone hsc70 is regulated by stress, cell signaling, and a composite targeting signal which is controlled by autoinhibition. *J. Biol. Chem.* **285**, 21858-21867.

Bermudez, V. P., Lindsey-Boltz, L. A., Cesare, A. J., Maniwa, Y., Griffith, J. D., Hurwitz, J. and Sancar, A. (2003). Loading of the human 9-1-1 checkpoint complex onto DNA by the checkpoint clamp loader hRad17-replication factor C complex in vitro. *Proc. Natl. Acad. Sci. USA* **100**, 1633-1638.

Bulavin, D. V., Higashimoto, Y., Popoff, I. J., Gaarde, W. A., Basrur, V., Potapova, O., Appella, E. and Fornace, A. J., Jr (2001). Initiation of a G2/M checkpoint after ultraviolet radiation requires p38 kinase. *Nature* **411**, 102-107.

Buschmann, T., Potapova, O., Bar-Shira, A., Ivanov, V. N., Fuchs, S. Y., Henderson, S., Fried, V. A., Minamoto, T., Alarcon-Vargas, D., Pincus, M. R. et al. (2001). Jun NH2-terminal kinase phosphorylation of p53 on Thr-81 is important for p53 stabilization and transcriptional activities in response to stress. *Mol. Cell. Biol.* **21**, 2743-2754.

Davis, R. J. (2000). Signal transduction by the JNK group of MAP kinases. *Cell* **103**, 239-252.

Delacroix, S., Wagner, J. M., Kobayashi, M., Yamamoto, K. and Karnitz, L. M. (2007). The Rad9-Hus1-Rad1 (9-1-1) clamp activates checkpoint signaling via TopBP1. *Genes. Dev.* **21**, 1472-1477.

Derheimer, F. A., O'Hagan, H. M., Krueger, H. M., Hanasoge, S., Paulsen, M. T. and Ljungman, M. (2007). RPA and ATR link transcriptional stress to p53. *Proc. Natl. Acad. Sci. USA* **104**, 12778-12783.

Dore, A. S., Kilkenny, M. L., Rzechorzek, N. J. and Pearl, L. H. (2009). Crystal structure of the rad9-rad1-hus1 DNA damage checkpoint complex–implications for clamp loading and regulation. *Mol. Cell* **34**, 735-745.

Dufault, V. M., Oestreich, A. J., Vroman, B. T. and Karnitz, L. M. (2003). Identification and characterization of RAD9B, a paralog of the RAD9 checkpoint gene. *Genomics* **82**, 644-651.

Foray, N., Marot, D., Gabriel, A., Randrianarison, V., Carr, A. M., Perricaudet, M., Ashworth, A. and Jeggo, P. (2003). A subset of ATM- and ATR-dependent phosphorylation events requires the BRCA1 protein. *EMBO J.* **22**, 2860-2871.

Francia, S., Weiss, R. S., Hande, M. P., Freire, R. and d'Adda di Fagagna, F. (2006). Telomere and telomerase modulation by the mammalian Rad9/Rad1/Hus1 DNA-damage-checkpoint complex. *Curr. Biol.* **16**, 1551-1558.

Guo, Z., Qian, L., Liu, R., Dai, H., Zhou, M., Zheng, L. and Shen, B. (2008). Nucleolar localization and dynamic roles of flap endonuclease 1 in ribosomal DNA replication and damage repair. *Mol. Cell. Biol.* **28**, 4310-4319.

Hopkins, K. M., Wang, X., Berlin, A., Hang, H., Thaker, H. M. and Lieberman, H. B. (2003). Expression of mammalian paralogues of HRAD9 and Mrad9 checkpoint control genes in normal and cancerous testicular tissue. *Cancer Res.* **63**, 5291-5298.

Hu, Z., Liu, Y., Zhang, C., Zhao, Y., He, W., Han, L., Yang, L., Hopkins, K. M., Yang, X., Lieberman, H. B. et al. (2008). Targeted deletion of Rad9 in mouse skin keratinocytes enhances genotoxin-induced tumor development. *Cancer Res.* **68**, 5552-5561.

Jiang, G. and Sancar, A. (2006). Recruitment of DNA damage checkpoint proteins to damage in transcribed and nontranscribed sequences. *Mol. Cell. Biol.* **26**, 39-49.

Karni-Schmidt, O., Zupnick, A., Castillo, M., Ahmed, A., Matos, T., Bouvet, P., Cordon-Cardo, C. and Prives, C. (2008). p53 is localized to a sub-nucleolar compartment after proteasomal inhibition in an energy-dependent manner. *J. Cell Sci.* **121**, 4098-4105.

Korgaonkar, C., Hagen, J., Tompkins, V., Frazier, A. A., Allamargot, C., Quelle, F. W. and Quelle, D. E. (2005). Nucleophosmin (B23) targets ARF to nucleoli and inhibits its function. *Mol. Cell. Biol.* **25**, 1258-1271.

Kruhlak, M., Crouch, E. E., Orlov, M., Montano, C., Gorski, S. A., Nussenzweig, A., Misteli, T., Phair, R. D. and Casellas, R. (2007). The ATM repair pathway inhibits RNA polymerase I transcription in response to chromosome breaks. *Nature* **447**, 730-734.

Lee, C., Smith, B. A., Bandyopadhyay, K. and Gjerset, R. A. (2005). DNA damage disrupts the p14ARF-B23(nucleophosmin) interaction and triggers a transient subnuclear redistribution of p14ARF. *Cancer Res.* **65**, 9834-9842.

Lee, J., Kumagai, A. and Dunphy, W. G. (2007). The Rad9-Hus1-Rad1 checkpoint clamp regulates interaction of TopBP1 with ATR. *J. Biol. Chem.* **282**, 28036-28044.

Leloup, C., Hopkins, K. M., Wang, X., Zhu, A., Wolgemuth, D. J. and Lieberman, H. B. (2010). Mouse Rad9b is essential for embryonic development and promotes resistance to DNA damage. *Dev. Dyn.* **239**, 2837-2850.

Liu, Z., Kenworthy, R., Green, C. and Tang, H. (2007). Molecular determinants of nucleolar translocation of RNA helicase A. *Exp. Cell Res.* **313**, 3743-3754.

Martindale, J. L. and Holbrook, N. J. (2002). Cellular response to oxidative stress: signaling for suicide and survival. *J. Cell Physiol.* **192**, 1-15.

Mayer, C. and Grummt, I. (2005). Cellular stress and nucleolar function. *Cell Cycle* **4**, 1036-1038.

Medhurst, A. L., Warmerdam, D. O., Akerman, I., Verwayen, E. H., Kanaar, R., Smits, V. A. and Lakin, N. D. (2008). ATR and Rad17 collaborate in modulating Rad9 localisation at sites of DNA damage. *J. Cell Sci.* **121**, 3933-3940.

Mendez, J. and Stillman, B. (2000). Chromatin association of human origin recognition complex, cdc6, and minichromosome maintenance proteins during the cell cycle: assembly of prereplication complexes in late mitosis. *Mol. Cell. Biol.* **20**, 8602-8612.

Pestov, D. G., Strezoska, Z. and Lau, L. F. (2001). Evidence of p53-dependent cross-talk between ribosome biogenesis and the cell cycle: effects of nucleolar protein Bop1 on G(1)/S transition. *Mol. Cell. Biol.* **21**, 4246-4255.

Rauen, M., Burtelow, M. A., Dufault, V. M. and Karnitz, L. M. (2000). The human checkpoint protein hRad17 interacts with the PCNA-like proteins hRad1, hHus1, and hRad9. *J. Biol. Chem.* **275**, 29767-29771.

Reinhardt, H. C., Aslanian, A. S., Lees, J. A. and Yaffe, M. B. (2007). p53-deficient cells rely on ATM- and ATR-mediated checkpoint signaling through the p38MAPK/MK2 pathway for survival after DNA damage. *Cancer Cell* **11**, 175-189.

Rendtlew Danielsen, J. M., Larsen, D. H., Schou, K. B., Freire, R., Falck, J., Bartek, J. and Lukas, J. (2009). HCLK2 is required for activity of the DNA damage response kinase ATR. *J. Biol. Chem.* **284**, 4140-4147.

Rubbi, C. P. and Milner, J. (2003). Disruption of the nucleolus mediates stabilization of p53 in response to DNA damage and other stresses. *EMBO J.* **22**, 6068-6077.

Scott, M., Boisvert, F. M., Vieyra, D., Johnston, R. N., Bazett-Jones, D. P. and Riabowol, K. (2001). UV induces nucleolar translocation of ING1 through two distinct nucleolar targeting sequences. *Nucleic Acids Res.* **29**, 2052-2058.

Thoms, H. C., Dunlop, M. G. and Stark, L. A. (2007). p38-mediated inactivation of cyclin D1/cyclin-dependent kinase 4 stimulates nucleolar translocation of RelA and apoptosis in colorectal cancer cells. *Cancer Res.* **67**, 1660-1669.

Toueille, M., El-Andaloussi, N., Frouin, I., Freire, R., Funk, D., Shevelev, I., Friedrich-Heineken, E., Villani, G., Hottiger, M. O. and Hubscher, U. (2004). The human Rad9/Rad1/Hus1 damage sensor clamp interacts with DNA polymerase beta and increases its DNA substrate utilisation efficiency: implications for DNA repair. *Nucleic Acids Res.* **32**, 3316-3324.

Unsal-Kacmaz, K., Makhov, A. M., Griffith, J. D. and Sancar, A. (2002). Preferential binding of ATR protein to UV-damaged DNA. *Proc. Natl. Acad. Sci. USA* **99**, 6673-6678.

Wang, X., Zou, L., Lu, T., Bao, S., Hurov, K. E., Hittelman, W. N., Elledge, S. J. and Li, L. (2006). Rad17 phosphorylation is required for claspin recruitment and Chk1 activation in response to replication stress. *Mol. Cell* **23**, 331-341.

Wang, Y., Chen, B., Li, Y., Zhou, D. and Chen, S. (2011). PNRC accumulates in the nucleolus by interaction with B23/nucleophosmin via its nucleolar localization sequence. *Biochim. Biophys Acta.* **1813**, 109-119.

Wansink, D. G., Schul, W., van der Kraan, I., van Steensel, B., van Driel, R. and de Jong, L. (1993). Fluorescent labeling of nascent RNA reveals transcription by RNA polymerase II in domains scattered throughout the nucleus. *J. Cell Biol.* **122**, 283-293.

Warmerdam, D. O., Freire, R., Kanaar, R. and Smits, V. A. (2009). Cell cycle-dependent processing of DNA lesions controls localization of Rad9 to sites of genotoxic stress. *Cell Cycle* **8**, 1765-1774.

Yang, J., Yu, Y., Hamrick, H. E. and Duerksen-Hughes, P. J. (2003). ATM, ATR and DNA-PK: initiators of the cellular genotoxic stress responses. *Carcinogenesis* **24**, 1571-1580.

Yogev, O., Saadon, K., Anzi, S., Inoue, K. and Shaulian, E. (2008). DNA damage-dependent translocation of B23 and p19 ARF is regulated by the Jun N-terminal kinase pathway. *Cancer Res.* **68**, 1398-1406.

Zhai, W. and Comai, L. (2000). Repression of RNA polymerase I transcription by the tumor suppressor p53. *Mol. Cell. Biol.* **20**, 5930-5938.

Zhang, Y., Ma, W. Y., Kaji, A., Bode, A. M. and Dong, Z. (2002). Requirement of ATM in UVA-induced signaling and apoptosis. *J. Biol. Chem.* **277**, 3124-3131.

Zou, L. and Elledge, S. J. (2003). Sensing DNA damage through ATRIP recognition of RPA-ssDNA complexes. *Science* **300**, 1542-1548.